

BLaDA: Bridging Language to Functional Dexterous Actions within 3DGS Fields

Fan Yang¹, Wenrui Chen^{1,2}, Guorun Yan¹, Ruize Liao¹, Wanjun Jia¹, Dongsheng Luo¹,
Kailun Yang^{1,2}, Zhiyong Li^{1,2}, and Yaonan Wang^{1,2}

Abstract—In unstructured environments, functional dexterous grasping calls for the tight integration of semantic understanding, precise 3D functional localization, and physically interpretable execution. Modular hierarchical methods are more controllable and interpretable than end-to-end VLA approaches, but existing ones still rely on predefined affordance labels and lack the tight semantic–pose coupling needed for functional dexterous manipulation. To address this, we propose BLaDA (Bridging Language to Dexterous Actions in 3DGS fields), an interpretable zero-shot framework that grounds open-vocabulary instructions as perceptual and control constraints for functional dexterous manipulation. BLaDA establishes an interpretable reasoning chain by first parsing natural language into a structured sextuple of manipulation constraints via a Knowledge-guided Language Parsing (KLP) module. To achieve pose-consistent spatial reasoning, we introduce the Triangular Functional Point Localization (TriLocation) module, which utilizes 3D Gaussian Splatting as a continuous scene representation and identifies functional regions under triangular geometric constraints. Finally, the 3D Keypoint Grasp Matrix Transformation Execution (KGT3D+) module decodes these semantic-geometric constraints into physically plausible wrist poses and finger-level commands. Extensive experiments on complex benchmarks demonstrate that BLaDA significantly outperforms existing methods in both affordance grounding precision and the success rate of functional manipulation across diverse categories and tasks. Code will be publicly available at <https://github.com/PopeyePxx/BLaDA>.

I. INTRODUCTION

Dexterous hands are the most crucial end-effectors of humanoid robots [1], [2]. To enable robots to interact with various objects in human environments and proficiently manipulate tools designed for humans, functional dexterous grasping is indispensable. Unlike conventional pick-and-place operations, functional grasping not only requires stable holding but also demands executing purposeful interactions on the correct functional part of an object with an understanding of task semantics [3]. This process involves fine-grained hand-object contact, pose-level constraints, and high-precision control,

This work was partially supported by the National Natural Science Foundation of China under Grants 62273137, 62473139, No. U21A20518, and No. U23A20341, the Hunan Provincial Research and Development Project under Grant 2025QK3019, the Hunan Science Fund for Distinguished Young Scholars under Grant 2024JJ2027, and the State Key Laboratory of Autonomous Intelligent Unmanned Systems (the opening project number ZZKF2025-2-10). (Corresponding author: Wenrui Chen.)

¹F. Yang, G. Yan, R. Rui, W. Jia, D. Luo, W. Chen, K. Yang, and Z. Li are with the School of Artificial Intelligence and Robotics, Hunan University, Changsha 410012, China. (E-mail: ysyf293@hnu.edu.cn, chenwenrui@hnu.edu.cn.)

²W. Chen, K. Yang, Z. Li, and Y. Wang are also with the National Engineering Research Center of Robot Visual Perception and Control Technology, Hunan University, Changsha 410082, China.

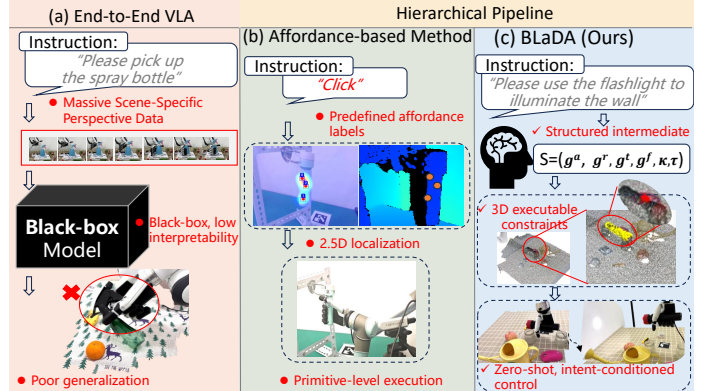


Fig. 1: Comparison of existing pipelines: (a) end-to-end VLA is data-hungry, black-box, and poor generalization; (b) affordance-based methods rely on predefined labels, limited 2.5D localization, and primitive control; (c) BLaDA (ours) uses a structured intermediate S with 3D executable constraints for zero-shot, intent-conditioned execution.

essentially relying on tightly coupled reasoning and cross-modal alignment among language understanding, environmental perception, and motor execution.

Early research works on functional grasping primarily relied on predefined task intentions [3], [4] or affordance semantics [5], [6], [7], [8] to assist in identifying interactive regions of objects. For instance, representative solutions [3], [9] have designed “touch-code” schemes that associate functional components with the palm or specific fingers based on preset intentions. However, these methods depend heavily on idealized perception systems, assuming that functional regions have been precisely segmented or localized—a requirement that is often difficult to meet in complex real-world environments [10]. Another category of research attempts to extract manipulation patterns directly from visual data. In this line, some studies [11], [12] have explored learning universal grasping strategies from human-object interaction videos. Moving further, affordance-based approaches [8], [13], [14] can identify key contact areas for grasping from limited category labels. For example, the Aff-Grasp system [13] implements a complete pipeline from automated data annotation to perceptual localization and parallel-jaw grasping. Nevertheless, the action modules of these methods typically still rely on independent general-purpose grasping models; affordance perception merely serves to narrow down candidate regions and fails to provide deterministic pose solutions for complex functional dexterous grasping. To address this gap between perception and action, a recent piece of research [10] has proposed a multi-keypoint affordance representation, establishing

a geometric link between visual features and manipulation actions by directly determining unique dexterous grasping poses.

Despite notable progress, existing approaches still face three major challenges toward general-purpose robotic manipulation (Fig. 1(b)). (i) Limited intent understanding: constrained by a closed instruction vocabulary and rigid semantic representations, systems generalize poorly to open-domain natural-language commands. (ii) Missing perceptual dimensionality: current affordance perception is largely confined to single-object localization in limited 2.5D scenes, and struggles in complex environments. (iii) Limited action execution: motion planning often stops at “grasping” itself, with insufficient consideration of subsequent intent execution.

The development of Large Language Models (LLMs) offers new directions. End-to-end Vision-Language-Action (VLA) models [15], [16], [17], [18], [19] can directly map language and perception to actions, but they are typically data-hungry, weakly interpretable, and brittle under distribution shift as shown in Fig. 1(a). Hierarchical pipelines [1], [20], [21] improve modularity by separating high-level planning from low-level control, yet they largely remain at basic grasping and fall short for functional dexterous grasping that requires tight semantic–pose coupling and finger-level precision. Even functionality-aware attempts such as SayFuncGrasp [22] still rely on learned planners to realize finger-level execution, leaving the semantics-to-action link weakly constrained and sensitive to the training distribution.

These observations motivate a key question: can we exploit the generalization and reasoning capability of foundation models by constructing a structured intermediate space that unifies language semantics, visual geometry, and motor control, enabling functional dexterous grasping across scenes and tasks? Achieving this goal entails three challenges: (1) how to design a unified protocol that bridges language, geometry, and control for generalizable and executable grasp planning; (2) how to go beyond 2D or sparse-3D affordance prediction to support pose-consistent, precise spatial reasoning; and (3) how to avoid a black-box mapping from semantics to actions, enabling physically interpretable and highly controllable execution.

To this end, we propose a modular zero-shot language-driven paradigm, BLaDA (Bridging Language to Dexterous Actions in 3DGS fields), which grounds open-vocabulary instructions into explicit perceptual and control constraints without task-specific policy training for semantic grounding. Following task decomposition, semantic alignment, and 3D executable representations, BLaDA establishes an interpretable reasoning chain from natural-language instructions to executable control, enabling object–part hierarchical localization in complex 3D scenes and intent-conditioned finger-level action generation (Fig. 1(c)).

Specifically, we first introduce a Knowledge-guided Language Parsing (KLP) module. In a zero-shot manner, KLP grounds open-vocabulary instructions into an explicit constraint interface by parsing them into a structured sextuple $\mathcal{S} = (g^a, g^r, g^t, g^f, t, k)$, covering available regions, finger-role assignments, grasp type, interaction force, task attributes, and topological knowledge. Inspired by instruction decomposi-

tion [14], KLP integrates an LLM with a structured knowledge graph, combining open-vocabulary understanding with domain priors to enable semantic-to-control conversion.

Next, we propose a learning-based Triangular Functional Point Localization (TriLocation) module. We adopt 3D Gaussian Splatting (3DGS) to build a continuous scene representation and design an object-part hierarchical feature extractor. Under a learnable triangular structural constraint anchored by (g_a, g_r, t, k) , TriLocation precisely identifies geometric subsets of functional regions in the Gaussian field, translating abstract “semantic-physical-contact” relations into pose-level spatial constraints.

Finally, we construct a 3D Keypoint Grasp Matrix Transformation Execution (KGT3D+) module. KGT3D+ decodes the semantic–geometric constraints into the final wrist pose and finger-level commands. Using contact keypoints estimated by TriLocation, it computes an optimal palm orientation and refines finger trajectories conditioned on grasp type g_t and force parameter g_f , thereby avoiding end-to-end black-box mapping and ensuring physically interpretable and precise execution.

To the best of our knowledge, this is the first research effort that investigates language-to-perception-to-action for dexterous functional manipulation. Our main contributions are summarized as follows:

- 1) A unified language-driven zero-shot framework, BLaDA, is proposed. By constructing a structured intermediate representation, it establishes an interpretable reasoning chain that unifies high-level instructions with low-level dexterous manipulation.
- 2) A structured semantic-geometric-control intermediate representation is introduced, and a sextuple produced by the KLP module is designed as a universal interface that connects cognitive semantics, visual perception, and motor control, thereby enabling cross-task transfer under open-vocabulary instructions.
- 3) Pose-level spatial constraints and a physically interpretable execution mechanism are proposed. The TriLocation and KGT3D+ modules are developed, where geometric structural constraints are incorporated within continuous 3D Gaussian fields, and geometric cues are mapped into physically meaningful action transformations, ensuring execution accuracy in complex tasks.
- 4) Extensive experimental validation is conducted: under a zero-shot setting, superior functional success rates and pose-consistency metrics are achieved by BLaDA on complex benchmark tests across multiple categories, tasks, and objects.

II. RELATED WORK

A. Affordance Grounding in 3D

Functional affordance modeling is a fundamental prerequisite for task-directed manipulation, requiring accurate identification and localization of semantically meaningful regions in 3D space. Traditional approaches based on RGB, RGB-D, or point cloud inputs [6], [7], [23] often suffer from resolution limitations, sparsity, or reliance on pre-defined

affordance classes, limiting their applicability in fine-grained manipulation. Additionally, the work of [24] introduces a language-conditioned imitation learning framework for long-horizon, multi-task manipulation. Recent advances in neural implicit representations [25] offer improved surface continuity, yet fall short in terms of real-time control and interpretability. 3D Gaussian Splatting (3DGS) [26] provides an efficient, continuous, and differentiable scene representation that combines high-fidelity geometry with rich appearance semantics. While prior works such as GaussianGrasper [27] and GraspSplats [28] demonstrate their potential for semantic segmentation and part localization, they remain limited to simple grasping settings like parallel-jaw grippers.

In this work, we extend 3DGS-based modeling to functional affordance grounding guided by natural language semantics, enabling precise, flexible, and generalizable grasp planning for dexterous manipulation.

B. Language-Guided Robotic Manipulation

Mapping natural language instructions to executable robotic actions has become a research hotspot in recent years. Existing approaches can be broadly categorized into two lines. One line adopts end-to-end Vision-Language-Action (VLA) learning [15], [16], [17], [18], [19], [29], where language, vision, and action are directly aligned through large-scale joint training. For instance, DexVLG [19] builds a large-scale dataset and trains a billion-parameter model to realize an end-to-end mapping from point clouds and instructions to dexterous hand poses; however, such methods are constrained by specific hardware setups and data-collection distributions, leading to performance degradation in unseen scenes. The other line follows a hierarchical pipeline [1], [20], [21]: a pre-trained Vision-Language Model (VLM) is used for high-level planning, and separate modules are then employed for low-level execution. Representative examples include ReKep [21], which parses instructions into path goals and sub-goal constraints, and DexGraspVLA [1], which combines domain-invariant features from foundation models with diffusion models to achieve general-purpose dexterous grasping. Nevertheless, these methods mostly focus on basic grasping and remain insufficient for functional grasping that requires deep semantic–pose coupling and finger-level fine-grained control.

The most related work, SayFuncGrasp [22], infers grasp functionality with LLMs but still relies on a trained policy planner to realize finger-level control, yielding a semantics-to-action mapping that is non-deterministic, weakly constrained, and sensitive to distribution shift. In contrast, we propose a structured primitive sextuple $S = (g^a, g^r, g^t, g^f, t, k)$ that parses language intent into executable perceptual and control constraints in a zero-shot manner, thereby reducing the reliance of semantic grounding on task-specific policy training and improving the stability of cross-scene generalization.

C. Object Representation for Dexterous Grasping

Conventional grasping approaches often rely on 6-DoF pose representations [30], [31], [32], [33], which are suitable for parallel-jaw grippers but insufficient to capture the multiple

contact points and complex hand-object interactions required for dexterous grasping. To address this, recent studies [34], [35], [3] have explored structure-aware functional representations. For instance, ContactDB [34] and the work of [3] have improved grasp performance by associating finger-level contacts with intent labels. However, these methods remain heavily dependent on high-precision perception systems and exhibit limited generalization.

To translate semantic localized regions into executable robotic actions, determining precise grasping directions and orientations is essential. Beyond indirect strategies like discretized orientation search [36], geometric analysis [37] offers a more direct mapping. Specifically, a representative approach [38] leverages Principal Component Analysis (PCA) on point clouds to achieve pose alignment based on geometric centroids and principal axes. Other methods, such as DexFuncGrasp [39] and MKA [10], model wrist-object contact as three-point constraints; however, these approaches often rely on depth-image-based reconstruction and struggle to handle perceptual localization in complex scenarios.

In contrast, we propose a novel paradigm based on 3D Gaussian Splatting (3DGS), which embeds grasp constraints directly into a dense geometric field, ensuring more robust functional localization and grasp synthesis.

III. METHODOLOGY

Problem Formulation This study aims to achieve functional dexterous grasping in a 3D reconstruction space based on natural language instructions from multiple perspectives. Specifically, the goal is to infer: (i) a set of three keypoint coordinates $P = \{p_1, p_2, p_3\}$ in 3D space on the target object, and (ii) a grasp configuration $G = (R, T, J, F)$ that defines the relative pose, joint state of the robotic hand and the force for execution.

Formally, the proposed framework \mathcal{M} takes as input a language instruction L and a collection of RGB-D images Ω , and outputs the grasp configuration G and keypoint set T as:

$$G, P = \mathcal{M}(L, \Omega).$$

Pipeline As shown in Fig. 2, our framework consists of three main stages: (1) Language parsing (the blue part in the figure), where the KLP module parses the input instruction L into a set of structured dexterous manipulation primitives $S = (g^a, g^r, g^t, g^f, t, k)$; see Sec. III-A for details. (2) Reconstruct 3D Gaussian Field and localization (the green part in the figure), where the TriLocation module first reconstructs the multi-view RGB observations into a 3D Gaussian field with object–part hierarchical semantic information, and then localizes three functional keypoints in the 3D Gaussian field conditioned on the parsed semantic anchors (g_a, g_r, t, k) ; see Sec. III-B. (3) Dexterous manipulation (the yellow part in the figure), where the FKG3D+ module generates the relative hand–object contact poses and incorporates semantic constraints (g_t, g_f) to produce fine-grained dexterous control actions; see Sec. III-C.

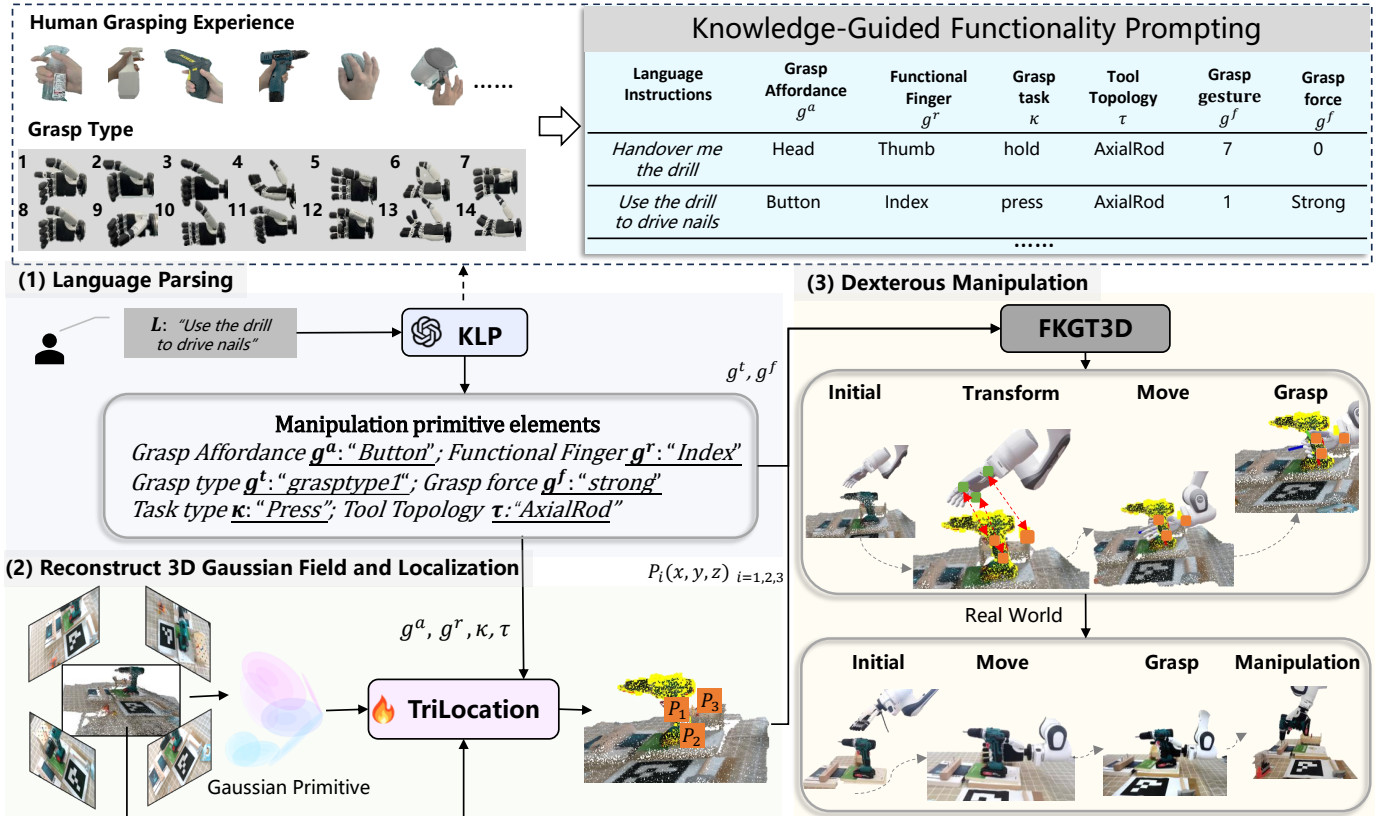


Fig. 2: Overview of BLADA. The top illustrates the construction of knowledge-guided functionality prompting and example demonstrations of “Handover me the drill” and “Use the drill”. The bottom shows the overall pipeline, which consists of three stages: (1) Language parsing (blue): the KLP module parses the input instruction L into structured manipulation primitive elements $\mathcal{S} = (g^a, g^r, g^t, g^f, \kappa, \tau)$; (2) 3D Gaussian reconstruction and localization (green): TriLocation reconstructs a semantic 3D Gaussian field from multi-view RGB observations and localizes three functional keypoints $P_i(x, y, z)$, conditioned on (g^a, g^r, κ, τ) ; (3) Dexterous manipulation (yellow): FKGT3D(+) generates relative hand–object contact poses and produces fine-grained dexterous control actions under semantic constraints (g^t, g^f) , which are finally executed in the real world.

A. Knowledge-guided Language Parsing (KLP)

To extract fine-grained, finger-level grasping constraints from an unstructured natural-language instruction L , we design a knowledge-guided language parsing module. Unlike prior approaches [8], [21] that rely solely on the general reasoning capability of large language models, our module explicitly injects domain priors into the reasoning chain and parses the instruction into a structured intermediate representation. This design aims to improve semantic consistency under diverse instruction styles and enhance robustness in open-vocabulary settings, thereby providing interpretable semantic anchors for subsequent perception and control.

Inspired by the work [14] on functional grasping, we decompose dexterous manipulation experience into four core primitives as the parsing scaffold. Specifically, g^a denotes the grasp affordance, which specifies the spatial reachability of usable regions on the object surface; g^r denotes role assignment, which clarifies the functional logic of each finger during contact; g^t denotes the grasp gesture/type, which directly corresponds to and stores the joint-angle values of different coarse hand postures; and g^f denotes the force level, which sets the interaction strength in the underlying dynamics.

During functional interaction in 3D space, there are often multiple plausible contact axes and execution paths. With-

out semantic disambiguation, downstream pose solving becomes under-constrained and exhibits multi-solution ambiguity, which may lead to unstable control. To address this issue, our parser further introduces a tool-topology prior τ and a task-intent prior κ as key constraints.

The tool-topology prior τ integrates geometric cues of tools with human operation habits and categorizes the target object into four topology classes: the axial-rod class τ_{rod} describes objects with a long-axis structure such as screwdrivers or knives; the lateral-handle class τ_{handle} corresponds to side-force structures such as spray bottles or kettles; the knob/wheel class τ_{knob} targets rotational interactive objects such as valves or door handles; and the slab/surface class τ_{surface} covers flat interactive interfaces such as computer mice, switches, or stapler shells. Such a topology abstraction provides structured constraints on action execution without requiring online geometric sensing. The task-intent prior normalizes verb phrases in the instruction and maps the action intent to four atomic task types press, click, open, hold. Here, press represents sustained-force actions such as pressing or squeezing; click corresponds to instantaneous triggering of a switch; open specifies opening operations that involve displacement or twisting; and hold is used for state-maintenance tasks such as holding, handover, or carrying. This prior is employed during parsing

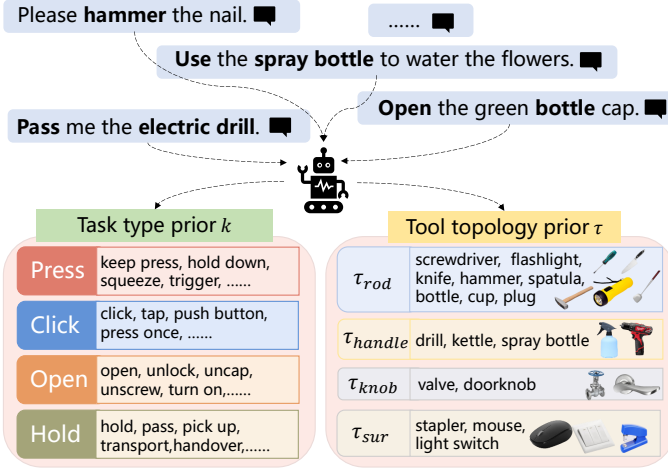


Fig. 3: Extract verbs, intent phrases, and tool types from human natural language instructions L , and classify them into specific task-intent priors and tool-topology priors.

to rule out logically inconsistent grasp combinations, ensuring that the produced semantic commitments are physically unique and feasible. As shown in Fig. 3, during the reasoning process, we can extract verbs, intent phrases, and tool types from human natural language instructions L , classifying them into specific task-intent priors and tool-topology priors, preparing for subsequent pose estimation.

We carefully design a prompt that contains three key components: (i) role specification: defining the execution context of the agent as an embodied intelligence; (ii) structured injection: providing the grasp taxonomy, task taxonomy, and tool-topology models from the F2F knowledge base to the model in a formalized manner; (iii) in-context examples: using representative “instruction–reasoning–tuple” exemplars to guide the model to output standardized results that comply with the downstream interface protocol.

Finally, given an instruction L and a knowledge prompt P , KLP maps them to a structured six-tuple representation:

$$\mathcal{S} = \{g^a, g^r, g^t, g^f, \tau, \kappa\} = \text{KLP}(L, P). \quad (1)$$

In implementation, KLP is driven by a large language model.

Prompt Design. The knowledge-guided prompt P comprises: (i) an *environment description* that fixes the agent role and execution objective (e.g., “You are a dexterous robot executing human instructions...”), (ii) *knowledge injection* that supplies structured functional grasp knowledge, the verb-task taxonomy, and the tool-topology taxonomy derived from F2F, and (iii) *few-shot exemplars* that demonstrate the desired six-tuple output format and succinct reasoning patterns.

B. Triangular Functional Point Localization Module (TriLocation)

Reconstructing a 3D Gaussian field with multi-level (object- and part-level) semantic information and localizing keypoints within it is crucial for bridging language and action. Multi-Keypoint Affordance (MKA) [10], learns interaction regions from web images and maps three key points of the object to corresponding locations on a dexterous hand, parameterizing a

single grasp with these three points. Inspired by MKA [10], we consider three contact points around the object: (1) a functional part point p_1 , corresponding to the functional fingertip contact (e.g., index finger or thumb); (2) a lateral support point p_2 , corresponding to the contact on the little-finger side; and (3) a wrist support point p_3 , representing the contact near the heel of the palm. These three points form a triangular structure that directly constrains the subsequent hand-object contact pose for dexterous grasping. Unlike MKA [10], which learns the locations of these three points in 2D images under weak supervision, we propose a TriLocation module (Fig. 4), which consists of three main steps: constructing 3D Gaussians with object-part features, localization of three functional keypoints, and constructing the local coordinate frame.

1) *Constructing 3D Gaussians with Object–Part Features:* While previous methods like GraspSplats [28] leverage large-scale vision models, e.g., CLIP [40] or SAM [41], they often suffer from semantic suppression, where large bounding boxes override smaller ones, and semantic drift, where localized cropping leads to a loss of global context. To address these issues, as shown in Fig. 4 (a), we introduce a Hierarchical Semantic Extraction (HSE) strategy, with the core being the select module and the context-aware cropping module.

Multi-granularity semantic mask generation. Given an input image I , we detect candidate bounding boxes $\{B_k\}_{k=1}^N$ via YOLO [42] and generate corresponding masks $\{M_k\}_{k=1}^N$ via SAM [41]. To prevent fine-grained semantics from being overwhelmed by object-level features, our select module decouples regions based on an area-ratio consistency hyperparameter α . Masks are categorized into an object-level set \mathcal{M}_o , representing large background or body regions, and a part-level set \mathcal{M}_p , representing localized functional components, according to whether the ratio of the mask area to its bounding box area exceeds α .

Context-aware part feature extraction. For object-level features, we extract a dense feature map $F_{co} \in \mathbb{R}^{C \times H \times W}$ from the full image. However, for part-level features, simple cropping of the part image I_{part} leads to semantic drift because the positional embeddings and attention mechanisms of CLIP [40] are highly sensitive to global context. To anchor the part semantics, we implement context-aware cropping. For each part box $B_p = [x_1, y_1, x_2, y_2]$, we expand the crop boundary by a padding ratio γ :

$$B'_p = [x_1 - \gamma w, y_1 - \gamma h, x_2 + \gamma w, y_2 + \gamma h], \quad (2)$$

where w, h are the width and height of B_p . The CLIP [40] encoder then processes this context-enriched crop. To obtain high-purity supervision signals, we perform a mask-guided projection that maps only the central features of the resulting feature map back onto the specific SAM [41] mask M_p . This ensures that the 3D Gaussian field learns high-resolution part details while maintaining the categorical context of the object.

Feature splatting and hierarchical distillation. We represent the scene using N 3D Gaussian primitives. Each Gaussian i carries a low-dimensional latent feature $\mathbf{f}_i \in \mathbb{R}^d$. Following the volumetric rendering scheme, the rendered latent feature

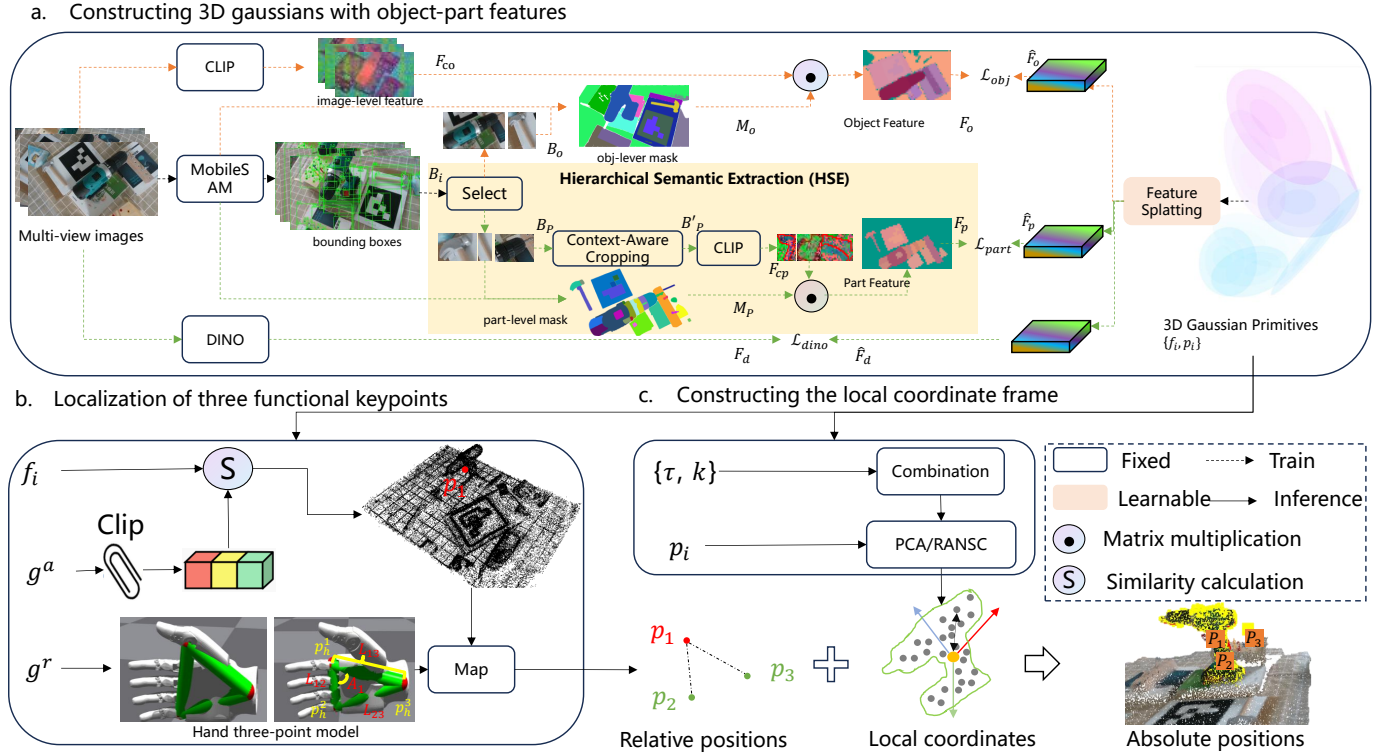


Fig. 4: Overview of the TriLocation. a. We design the HSE module (highlighted in yellow), consisting of Select and Context-Aware Cropping units to decouple object/part regions and resolve semantic drift. This enables the construction of a clean, high-precision 3D Gaussian semantic field for keypoint localization. b. The module computes the CLIP [40] similarity between g^a and each Gaussian feature f_i to locate the semantic anchor p_1 . c. A lightweight MLP predicts two relative offsets Δp_2 and Δp_3 , forming the graspable triangle structure $\{p_1, p_2, p_3\}$, which is supervised by structure-aware losses based on edge lengths and internal angles.

$\hat{\mathbf{F}}$ is obtained as:

$$\hat{\mathbf{F}} = \sum_{i=1}^N \mathbf{f}_i \alpha_i \prod_{j=1}^{i-1} (1 - \alpha_j). \quad (3)$$

A shallow MLP then decodes $\hat{\mathbf{F}}$ into object-level (\hat{F}_o), part-level (\hat{F}_p), and DINO-v2 (\hat{F}_d) branches.

Background consistency constraint. To maximize the signal-to-noise ratio and prevent energy leakage into background regions, we enforce a hard mask-guided constraint during the preprocessing stage. For pixels i that do not belong to any detected masks at the corresponding level, we explicitly set the ground-truth feature vector to zero:

$$F_s^*(i) = \mathbf{0}, \quad \text{if } i \notin \Omega_s, \quad (4)$$

where Ω_s is the union of all masks at level s . By distilling from these clean, masked feature maps, the 3D Gaussian field naturally learns to suppress responses in non-target regions. The overall objective remains $L = L_{obj} + L_{part} + \lambda L_{dino}$.

2) *Localization of Three Functional Keypoint:* After constructing the multi-level semantic 3D Gaussian field, we localize the three functional keypoints in 3DGS based on the output of KLP, as illustrated in Fig. 4 (b). First, the grasp-region semantics g^a is fed into CLIP [40] to obtain a query vector, which is compared with the semantic feature f_i of each Gaussian in the field to compute the similarity S , forming a similarity distribution. Gaussian points with similarity higher than a threshold δ are clustered in 3D space, and the centroid

of the cluster with the highest confidence is selected as the semantic anchor p_1 on the object.

Next, the grasp-relation semantics g^r is fed into the Hand three-point model to select a functional hand template that contains the three hand keypoints p_{h1}, p_{h2}, p_{h3} . The Map module then uses the task-topology local coordinate frame (introduced in Sec. III-B3) to rigidly align this predefined three-point hand template to the object space: using the semantic anchor p_1 as the alignment reference, the functional fingertip p_{h1} , little-finger point p_{h2} , and wrist point p_{h3} in the hand template are rotated and translated to correspond to p_1, p_2, p_3 on the object, respectively. Specifically, taking p_1 as the origin and $(\hat{x}, \hat{y}, \hat{z})$ as the task-topology local coordinate frame, we construct a triangle in this local frame: p_3 is fixed along the $-z$ direction, and p_2 lies in the $y-z$ plane, forming an angle A_1 with p_3 . Let (L_{12}, L_{13}, L_{23}) be the edge lengths provided by the template; then the world coordinates of p_2 and p_3 are given by

$$\mathbf{p}_2 = \mathbf{p}_1 + R \begin{bmatrix} 0 \\ -L_{12} \sin A_1 \\ -L_{12} \cos A_1 \end{bmatrix}, \quad \mathbf{p}_3 = \mathbf{p}_1 + R \begin{bmatrix} 0 \\ 0 \\ -L_{13} \end{bmatrix},$$

where $R \in \mathbb{R}^{3 \times 3}$ is the rotation matrix determined by the task-topology rules, whose column vectors correspond to the local axes $(\hat{x}, \hat{y}, \hat{z})$ expressed in the world coordinate frame.

3) *Constructing the local coordinate frame:* In the $SE(3)$ space, pose estimation often suffers from ambiguity, as relying solely on point-level geometric information can lead to redundant or mirrored contact configurations. To address

TABLE I: Definition of Local Coordinate Frames under Task-Tool Topology Constraints. The frame follows the right-hand rule where $\hat{x} = \hat{y} \times \hat{z}$.

Task Intent κ	Tool Topology τ	\hat{z} (Primary Axis)	\hat{y} (Hand Orientation)
Hold	τ_{rod}	Gravity Direction	Structural Axis
	τ_{handle}	Radial Direction	Handle Axis
	τ_{knob}	Surface Normal	Tangential Direction
	τ_{surface}	Surface Normal	Major In-plane Axis
Press	τ_{handle}	Tool Forward Axis	Handle Axis
Open	τ_{knob}	Rotation Axis	Tangential Direction
Click	τ_{surface}	Click Normal	Major In-plane Axis
	τ_{rod}	Click Normal	Major In-plane Axis

this, we construct a local coordinate frame constrained by the coupling of task semantics and tool topology (as shown in Fig. 4(c)), providing a task-consistent geometric reference for contact reasoning.

First, we couple the task-intent prior κ with the tool-topology prior τ . As defined in Table I, we specify a primary task axis \hat{z} and a hand orientation axis \hat{y} for each combination. To automatically estimate these geometric primitives from raw point clouds, we employ robust fitting strategies tailored to different topologies: the Random Sample Consensus (RANSAC) [43] algorithm is utilized to extract the structural axes of axial rods or lateral handles (serving as rod/handle axes) as well as the rotation axes of knobs; Principal Component Analysis (PCA) [44] is applied to estimate the surface normals of slab-like structures as the \hat{z} axis, with the first principal component extracted as the major in-plane axis. Furthermore, we synthesize task-driven features, including a radial direction for determining grasp depth and a tool forward axis identified through the global distribution of the point cloud.

After determining the initial vectors, we project \hat{y} onto the plane orthogonal to \hat{z} to eliminate non-orthogonal components, thereby ensuring the stability of the coordinate frame. Finally, the complete hand-aligned coordinate frame $(\hat{x}, \hat{y}, \hat{z})$ is obtained via $\hat{x} = \hat{y} \times \hat{z}$. This frame provides a consistent, right-handed reference for defining the wrist point p_3 , the functional finger point p_1 , and the supportive finger point p_2 .

C. Keypoint-based Grasp matrix Transformation in 3D for Dexterous Execution (KGT3D+)

The KGT3D+ module is an extension and enhancement of the Keypoint-to-Grasp-Template (KGT) method proposed in MKA [10], designed to generate physically executable 3D grasp control commands. Compared with the original KGT method, which estimates grasp poses using keypoints and pre-defined templates, KGT3D+ introduces a complete 3D spatial pose construction pipeline and augments the framework with finger joint and force-level control parameters. This enables an end-to-end grasp execution process, from contact structure perception to fine-grained motion control.

After receiving the three key points $\{p_1, p_2, p_3\}$ on the object, KGT3D+ first constructs an accurate palm pose (R, T) . Specifically, we take p_3 as the palm reference point and

construct a right-handed coordinate frame to represent the wrist pose in 3D space. The axes are defined as:

$$\vec{z} = \frac{p_1 - p_3}{\|p_1 - p_3\|}, \quad \vec{y} = \frac{(p_2 - p_3) \times \vec{z}}{\|(p_2 - p_3) \times \vec{z}\|}, \quad \vec{x} = \vec{y} \times \vec{z}. \quad (5)$$

The resulting wrist pose is given by:

$$R = [\vec{x} \ \vec{y} \ \vec{z}], \quad T = p_3. \quad (6)$$

Here, $R \in \mathbb{R}^{3 \times 3}$ denotes the wrist rotation matrix, and $T \in \mathbb{R}^3$ is the translation vector.

Meanwhile, the grasp type g^t and force label g^f from the language parsing module are passed into a predefined functional grasp library (F2F) [14], which maps them to the joint configuration J and per-finger force profile F :

$$J, F = \text{F2F}(g^t, g^f), \quad (7)$$

where J describes the joint angles of the robotic hand, and F represents the desired force distribution across fingers.

IV. EXPERIMENTS

In this section, we conduct comprehensive experiments to evaluate our proposed framework across three key components. First, we assess the KLP module’s ability to extract fundamental manipulation elements from natural language. Second, we evaluate the TriLocation module for generating semantically grounded and geometrically valid contact keypoints. Finally, we demonstrate the full system’s capability in real-world end-to-end manipulation tasks, where the KGT3D+ module converts contact keypoints into executable grasp poses with joint and force control, enabling functional execution without task-specific training.

A. Setup

1) *Scenes, Objects, and Devices*: Our experimental setup is illustrated on the left side of Figure 5. It comprises a Franka Emika robot arm equipped with a 6-DOF (degree-of-freedom) dexterous Inspire Hand for executing grasping tasks, and an Intel RealSense D435i camera for multi-view image acquisition. We configured over 10 open tabletop scenarios using 18 types of tools from the representative dexterous grasping datasets FAH [14], [45]. Six typical scenarios are showcased on the right of Fig. 5, based on which a total of 100 language-guided manipulation trials were conducted. An NVIDIA RTX 3090 GPU was utilized for 3D reconstruction and the training of the TriLocation module.

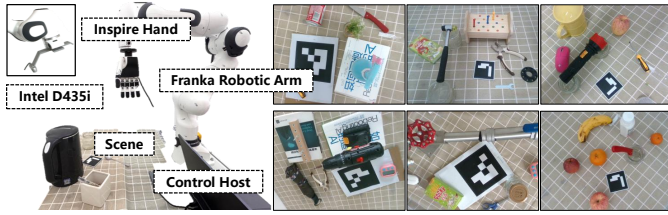


Fig. 5: Real-world experiment setting and 6 typical scenarios demonstration.

2) *Evaluation Metrics*: To comprehensively evaluate the system performance, we establish a progressive evaluation framework: it begins with the assessment of language reasoning accuracy, followed by the measurement of 2D part-level feature extraction precision, then the verification of 3D keypoint localization compliance, and finally the evaluation of physical execution success rate via real-world trials.

For consistent mathematical notation, let P and G denote the predicted and ground-truth affordance heatmaps, respectively, and M be the binary mask of the target part. Let P_i , G_i , and M_i represent the i -th pixel values, with N being the total number of pixels. The specific metrics are defined as follows:

- **Language Reasoning Accuracy (LRA)**: Evaluates the correctness of the system in inferring fundamental manipulation elements from natural language instructions. It is defined as the ratio of correctly inferred cases to the total number of test cases.
- **2D Part-level Localization Metrics**: To quantitatively evaluate the precision of 2D part-level feature extraction used to constrain 3D rendering, we adopt the following metrics:
 - **Mean Absolute Error (MAE)**: Measures the pixel-wise average deviation between P and G : $MAE = \frac{1}{N} \sum_{i=1}^N |P_i - G_i|$.
 - **Precision Energy (P_{En})**: Quantifies the concentration of predicted energy within the target part mask M : $P_{En} = \frac{\sum P_i M_i}{\sum P_i}$.
 - **Affordance Grounding Metrics**: Following [6], [7], we introduce KL Divergence (KLD), Similarity (SIM), and Normalized Scanpath Saliency (NSS) to assess the distributional alignment between the predicted heatmaps and the ground-truth part regions.
- **Localization Success Rate (LSR)**: Whether the 3D coordinate deviations between keypoints are within predefined thresholds.
- **Functional Grasp Success Rate (FSR)**: It measures the proportion of successful functional grasping tasks completed during physical trials.

B. KLP-Based Language Parsing Evaluation

To assess the contribution of external knowledge, we evaluate three representative large language models: ChatGPT4.0 [46], DeepSeekv3 [47], and Gemini2.5 [48], under two configurations: with the proposed Knowledge-Guided Language Parsing (KLP) module and without it.

TABLE II: Comparison of LLMs w/ and w/o KLP on Language Reasoning Accuracy (LRA). Best results are in bold.

Model	g^a	g^t	g^f	g^r	t	k	Avg.
ChatGPT4.0 [46] (w/)	0.65	0.81	0.74	0.74	0.72	0.86	0.753
ChatGPT4.0 [46] (w/o)	0.43	0.13	0.45	0.51	0.72	0.81	0.508
DeepSeekv3 [47] (w/)	0.62	0.80	0.74	0.79	0.73	0.78	0.743
DeepSeekv3 [47] (w/o)	0.42	0.18	0.46	0.62	0.77	0.79	0.540
Gemini2.5 [48] (w/)	0.70	0.85	0.64	0.80	0.66	0.82	0.745
Gemini2.5 [48] (w/o)	0.51	0.22	0.50	0.65	0.59	0.78	0.542

The evaluation is conducted on six manipulation elements (g^a, g^t, g^f, g^r, t, k) using Language Reasoning Accuracy (LRA) as the metric.

As shown in Table II, three key observations can be made:

Consistent improvement across all models. Integrating the KLP module significantly enhances performance for all three LLMs. The average LRA increases from 0.508 \rightarrow 0.753 for ChatGPT4.0 [46], 0.540 \rightarrow 0.743 for DeepSeekv3 [47], and 0.542 \rightarrow 0.745 for Gemini2.5 [48], corresponding to an average relative gain of approximately +21.5%. This confirms that KLP serves as a robust, plug-and-play reasoning module adaptable to diverse LLM architectures.

Largest gains are observed in task- and function-related elements. The most substantial improvements occur in g^t and g^r , which correspond to the grasp type and the functional finger, respectively. Both elements inherently require domain-specific expertise to make correct predictions. Purely language-based reasoning is insufficient in these cases. For instance, ChatGPT4.0 [46]’s g^t accuracy improves dramatically from 0.13 to 0.81 (+0.68), while Gemini2.5 [48] achieves the best g^r accuracy of 0.80. These results highlight that structured knowledge integration plays a decisive role in enabling precise functional reasoning and semantic alignment in manipulation tasks.

ChatGPT4.0 [46] (w/ KLP) achieves the best overall performance. Among all models, ChatGPT4.0 [46] (w/ KLP) attains the highest average LRA of 0.753, achieving top results in four out of six elements. This indicates ChatGPT4.0 [46]’s stronger capability to exploit structured knowledge for task reasoning and manipulation-oriented language understanding.

Overall, these results demonstrate that the proposed KLP module can act as a generalizable and lightweight plug-in, consistently improving structured language grounding across various LLM backbones.

C. Performance Evaluation of TriLocation

We evaluate the proposed TriLocation module from both qualitative visualization and quantitative analysis, and verify its effectiveness and advantages in two aspects: part-level feature extraction and three-dimensional localization of functional keypoints.

Qualitative comparison. First, we conduct a qualitative comparison with the GraspSplats [28] baseline on object-/part-level semantic feature rendering to verify the effectiveness of the proposed Hierarchical Semantic Extraction (HSE) module. As shown in Fig. 6, GraspSplats [28] tends to suffer



Fig. 6: Relevance maps of given language instructions. We project the language-activated 3D Gaussian semantic features onto 2D images for visualization. The orange panels denote object-level relevance maps, while the green panels denote part-level relevance maps. Red rectangles highlight the erroneous or ambiguous responses of GraspSplats, and yellow ellipses indicate that our method produces more compact and complete response regions for local semantic parts.

from semantic “cross-talk” at the object level (orange boxes), activating irrelevant yet semantically similar regions (e.g., querying “drill” also highlights a knife-like object). At the part level (green boxes), it exhibits an evident “holistic override” effect, where part queries often diffuse to the entire object (e.g., “hammer-handle” nearly highlights the whole hammer), leading to blurred boundaries and unstable localization. In contrast, our method delineates clearer object and part contours in the same scenes, with more compact and complete responses for fine-grained parts. This advantage mainly stems from the HSE module, which explicitly filters and decouples object-level and part-level features, mitigating the issue in GraspSplats [28] where part representations are overwhelmed by global object semantics. Consequently, our rendering provides a more reliable prior for subsequent part-level semantic queries and functional region localization in the 3D Gaussian field.

Second, we qualitatively visualize the role of the proposed local coordinate system in 3D functional keypoint localization. As shown in Fig. 7, we present representative results of four typical task-tool combinations across three scenes. Each group includes, in order, an input image used for reconstruction, a 3D visualization of the constructed local coordinate system, the predicted three-point configuration with the local coordinate constraint, and the prediction without the local coordinate constraint (highlighted with red boxes). Without a stable spatial reference frame, the variant w/o local coordinate often yields disordered triangular structures and semantic misalign-

TABLE III: Quantitative comparison of 2D Part Localization Performance. Our method shows significant improvements in localization accuracy and energy focus across different object scales.

Query Item	Model	MAE ↓	P_En ↑	KLD ↓	SIM ↑	NSS ↑
Hammer Handle	GraspSplats [28]	0.0141	0.2798	14.1642	0.1449	1.2916
	Ours	0.0127	0.5962	13.0819	0.2040	2.7209
<i>Improvement</i>		(9.9%)	(113.1%)	(7.6%)	(40.8%)	(110.7%)
Spray Bottle	GraspSplats [28]	0.0028	0.4001	12.7509	0.2529	7.9788
	Ours	0.0028	0.4134	12.5954	0.2534	8.0849
<i>Improvement</i>		(0.0%)	(3.3%)	(1.2%)	(0.2%)	(1.3%)

ment among the three points, making their absolute layouts unreliable for providing consistent and correct approach and interaction directions for functional grasping. For example, in the “Hold Drill” and “Open Bottle” cases, the wrist contact point p_3 should be located on the upper side according to the task semantics to support a stable approach, yet the unconstrained variant incorrectly places it on the lateral side, which compromises downstream executable grasp/operation poses. In contrast, our method learns a structure-adaptive local coordinate system in the multi-view 3D Gaussian field, enabling the three keypoints to preserve a stable geometric triangle and a semantically consistent spatial configuration across different viewpoints, object topologies, and task semantics.

Quantitative evaluation. We evaluate the proposed module

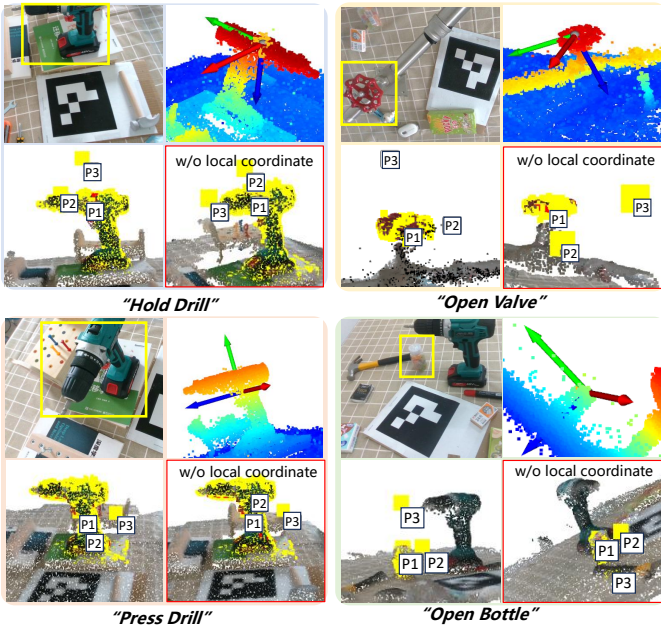


Fig. 7: Visualization of the effect of the local coordinate system on 3D functional keypoint localization. Each example presents, in order: the input image, a 3D visualization of the local coordinate system (red/green/blue indicate the $x/y/z$ axes, where blue denotes the approach axis z and green denotes the grasp axis y), the predicted three-point structure under the local-coordinate constraint, and the results without this constraint (red boxes).

TABLE IV: Quantitative comparison of LSR (%) across 4 task categories and ablation variants.

Method	Hold	Press	Open	Click	Mean LSR
MKA [10]	50	20	10	10	22.5
w/o Local Coordinate	50	0	0	50	25
w/o HSE Module	62.5	50	50	50.0	53.13
TriLocation (Ours)	75	50	100	50	68.75

through two dimensions: part-level semantic query performance and 3D functional keypoint localization accuracy.

First, we quantitatively evaluate the positioning accuracy of part-level semantic queries. As shown in Table III, our proposed enhancements achieve significant improvements across all evaluation metrics compared to the baseline method, GraspSplats [28]. For queries targeting relatively large components such as the ‘‘Hammer Handle’’, the Precision Energy (P_{En}) increased substantially from 0.2798 to 0.5962 (a 113.1% improvement), and the Normalized Scan Saliency (NSS) grew by 110.7%. These results indicate that the part-level heatmaps generated by our method exhibit exceptionally high focus, effectively addressing the issues of feature diffusion and background interference prevalent in the original method. Simultaneously, for queries involving fine-grained, extremely small parts like the ‘‘Pink Button of the Spray Bottle’’, our method maintains superior MAE and KLD scores. The experimental data fully demonstrate that by introducing the HSE module, the localization precision and spatial consistency of

fine-grained parts across various scales can be significantly enhanced within 3D Gaussian Splatting (3DGS) scenarios.

Following the evaluation protocol of GaussianGrasper [27], we adopt *Localization Success Rate* (LSR) as the core metric. A localization is considered successful only when the predicted three-point topological structure simultaneously satisfies the required grasp positions and the task-specific geometric functional constraints.

We evaluate our method across 6 typical real-world scenes as shown in Fig. 5, covering 14 representative task-tool combinations categorized into four functional intents: *Hold* (including knife, spray bottle, drill, umbrella, hammer, pliers, bottle, and flashlight), *Press* (drill and spray bottle), *Open* (valve and bottle), and *Click* (flashlight and mouse).

As shown in Table IV, TriLocation achieves a robust overall LSR of 68.75%. Notably, the baseline method MKA [10] lacks open-vocabulary semantic query capabilities and requires manual point-clicking to identify functional parts. To obtain its evaluation results, each task-tool combination was tested 10 times to record the data, whereas our TriLocation requires only a single trial per combination to achieve stable localization. Despite the manual assistance and multiple trials, MKA [10]’s overall LSR remains limited to 22.5%, primarily due to its susceptibility to depth errors during the 2D-to-3D lifting process in complex environments.

Ablation studies further highlight the necessity of our proposed modules. Without the task-topology local coordinate frame constraint, the system fails to resolve the orientation for critical tasks like ‘‘Press’’ and ‘‘Open’’ (dropping to 0% success rate in these categories), causing the mean LSR to drop sharply to 25%. Similarly, removing the Hierarchical Semantic Extraction (HSE) module leads to a decrease in LSR to 53.13%, as fine-grained part features become blurred by global object context. These results demonstrate that the integration of hierarchical mask constraints and task-topology reasoning effectively suppresses feature diffusion and ensures the high precision and spatial consistency of 3D fine-grained keypoint localization.

Hyperparameter Analysis. We evaluate the sensitivity of our module to the area-ratio consistency $\alpha \in \{0.05, \dots, 0.6\}$ and padding ratio $\gamma \in \{0.1, \dots, 0.6\}$. As shown in Table 9, we record the MAE and P_{En} using the ‘‘Flashlight Button’’ as a representative fine-grained query.

The results indicate that the optimal performance is achieved at $(\alpha = 0.1, \gamma = 0.4)$, yielding the lowest MAE (0.0040) and highest P_{En} (0.3134). We observe that a moderate padding ratio ($\gamma = 0.4$) provides essential spatial context for the CLIP [40] encoder, effectively suppressing semantic drift. However, excessively large values ($\gamma = 0.6$) introduce background noise that contaminates the part features. Furthermore, the performance remains effective for $\alpha \leq 0.15$, but significantly degrades when $\alpha \geq 0.3$, suggesting that an overly restrictive area-ratio threshold might lead to the loss of critical part-level semantic information.

D. BLaDA Performance in Real-world Environments

Fig. 8 presents qualitative results of our system executing natural-language tasks in real-world environments. The in-

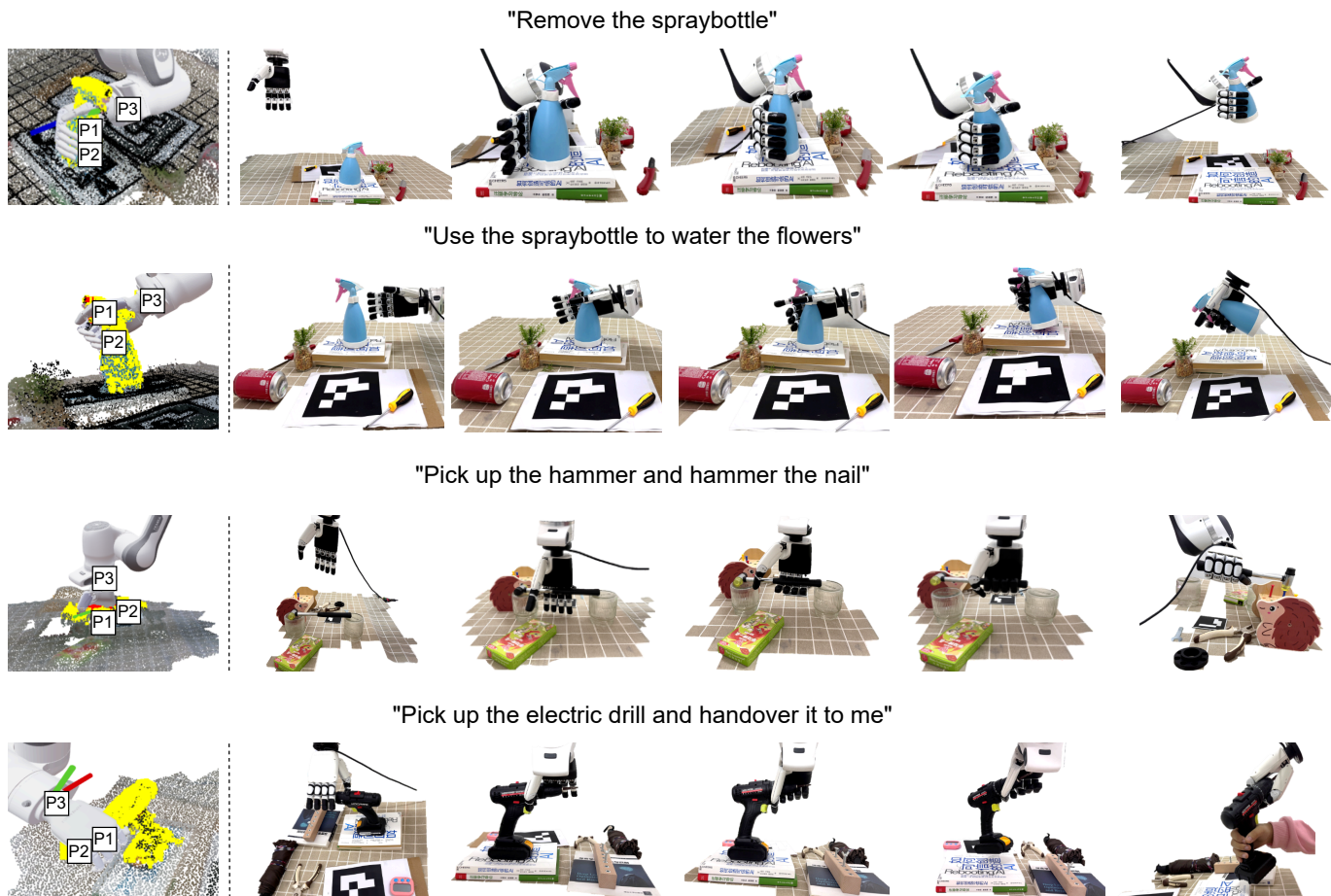


Fig. 8: Dexterous grasping demonstration workflow based on 3D reconstructed points. Left of the dashed line: predicted reference points. Right of the dashed line, in sequence: initial state; pose alignment; coarse grasping based on g^t ; tightening non- g^f fingers; and g^f fingers exerting g^r force (Note that, except for the finger-force actuation, the post-grasp motions are completed by demonstration).

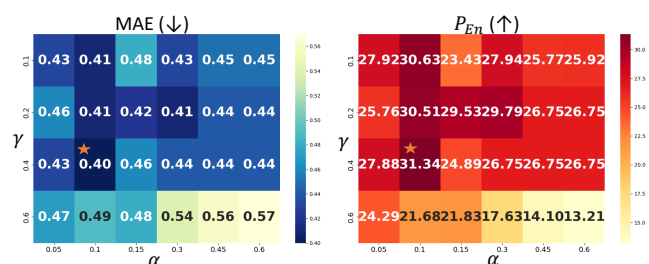


Fig. 9: Hyperparameter analysis of α and γ . The optimal configuration is highlighted.

structions range from simple object relocation to tool-level functional manipulation, including “Remove the spraybottle” (first row of Fig. 8) as well as “Use the spraybottle to water the flowers”, “Pick up the hammer and hammer the nail”, and “Pick up the electric drill and handover it to me” (last three rows of Fig. 8). As shown in Fig. 8, we first generate object grasp poses (Q, T) on 3DGS via KGT3D+ (first column), and drive the real robot to move from the initial pose (second column) to the target grasping position (third

TABLE V: FGS (%) on two real-world task-tool combinations (5 trials each).

Task-Tool	Ours	MKA [10]	DP* [49]
Hold Spraybottle	80	40	50
Press Spraybottle	30	10	10

column). The KLP module then outputs g^t to produce coarse grasp gesture joint angles J and perform the initial enclosure (fourth column), followed by g^r to tighten the remaining four fingers for improved stability (fifth column). Finally, g^f drives the functional finger to execute task-specific operations (sixth column). For example, in the watering task, the robot presses the index finger after reaching above the plant to trigger spraying. These results indicate that our method can stably extract the “task-function-part-finger” elements from open-domain instructions and ground them into topology/semantics-constrained grasps and functional actions, enabling closed-loop generalization from “understanding” to “execution”.

Comparative Analysis. To verify the effectiveness of the proposed method under real-world manipulation conditions, this section selects two representative task-tool combinations,

namely “hold the spray bottle” and “press the spray bottle,” for comparative experiments. In selecting baseline methods, this chapter follows the principle of prioritizing output comparability; that is, the included methods must be able to generate executable control outputs for functional dexterous grasping on the same hardware platform, including wrist pose as well as multi-finger joint motions / functional finger actions, and must be applicable to tool-oriented functional manipulation tasks. Based on this criterion, the MKA method [10] is adopted as the functional grasping baseline, and the end-to-end policy DP* is introduced as a data-driven direct mapping baseline. Specifically, DP* extends Diffusion Policy [49] by adding a prediction head for the 6-DoF dexterous hand joint control, and is trained or fine-tuned using 20 teleoperation / data-glove demonstration trajectories collected for each task category. All methods are evaluated under the same sensing configuration and testing scenarios, and all take affordance-type instructions (e.g., “hold,” “press”) as input. Each task-tool combination is tested in 5 independent trials, and the average results are reported in Table V.

From the overall results, the proposed method achieves the best performance on both tasks. In the “hold the spray bottle” task, the success rate of our method reaches 80%, outperforming MKA (40%) and DP* (50%) by 40 and 30 percentage points, respectively. In the more challenging “press the spray bottle” task, our method achieves a success rate of 30%, whereas both MKA and DP* only achieve 10%. These results indicate that the proposed method not only exhibits higher execution reliability in stable holding scenarios but also demonstrates a more pronounced advantage in high-precision manipulation tasks that require accurate component alignment and functional finger triggering.

Further analysis shows that MKA attains only a 10% success rate on the “press” task, mainly because it relies heavily on single-object scenes and structured environments. In real environments with multiple objects, interference, and occlusions, its stability in locating and aligning key functional components degrades significantly. In contrast, DP* achieves a 50% success rate on the “hold” task, but drops to 10% on the “press” task, indicating that end-to-end direct mapping policies remain sensitive in terms of fine contact alignment and cross-scene generalization. This demonstrates that, compared with baseline methods relying on structural scene assumptions or task-specific training, the zero-shot grasping mechanism with explicit semantic and geometric constraints exhibits stronger adaptability and stability in open environments.

In summary, the results in Table V validate the robustness, precision, and generalization capability of the proposed functional dexterous grasping method in real-world tasks. By simply capturing multi-view images of the scene to perform 3D reconstruction, and utilizing explicit semantic constraints, geometric constraints, and a unified 3D representation, the proposed method stably maps key execution elements from open-domain instructions into executable grasping and functional actions. Consequently, it achieves superior performance in both simple holding and high-precision pressing tasks in a zero-shot manner, significantly reducing data collection and training costs.

V. CONCLUSIONS AND FUTURE WORK

We propose a zero-shot functional dexterous grasping framework for 3D open scenes that bridges language, vision, and action. Unlike data-intensive end-to-end models, this method employs a modular architecture combined with 3D Gaussian fields to directly map natural language instructions into physically executable actions, eliminating the need for task-specific training. The framework integrates three core components: knowledge-guided semantic parsing to extract interpretable manipulation constraints, geometry-aware triangular reasoning to achieve robust functional region localization, and 3D grasp matrix transformations to generate executable wrist and finger-level control commands. These designs significantly enhance the system’s generalization capability, localization accuracy, and grasp success rate in complex environments, providing a unified, scalable, and practically deployable solution for real-world functional manipulation.

However, the current system’s reliance on 3DGS-based semantic fields still faces challenges due to sparse and imprecise fine-grained understanding; existing vision-language models often exhibit semantic ambiguity when parsing tool components, such as misinterpreting a tool’s “head” or “body” as anatomical human parts. Furthermore, the lack of haptic feedback makes the system sensitive to unexpected object displacement or slippage during the grasping process. Future research will focus on enhancing part-level semantic density and integrating tactile sensors to achieve closed-loop adjustment and more robust dynamic human-robot interaction.

REFERENCES

- [1] Y. Zhong *et al.*, “DexGraspVLA: A vision-language-action framework towards general dexterous grasping,” *arXiv preprint arXiv:2502.20900*, 2025.
- [2] C. Guo *et al.*, “Grasp like humans: Learning generalizable multi-fingered grasping from human proprioceptive sensorimotor integration,” *IEEE Transactions on Robotics*, vol. 41, pp. 5700–5719, 2025.
- [3] T. Zhu, R. Wu, J. Hang, X. Lin, and Y. Sun, “Toward human-like grasp: Functional grasp by dexterous robotic hand via object-hand semantic representation,” *IEEE Transactions on Pattern Analysis and Machine Intelligence*, vol. 45, no. 10, pp. 12 521–12 534, 2023.
- [4] S. Brahmabhatt, A. Handa, J. Hays, and D. Fox, “ContactGrasp: Functional multi-finger grasp synthesis from contact,” in *Proc. IROS*, 2019, pp. 2386–2393.
- [5] A. Myers, C. L. Teo, C. Fermüller, and Y. Aloimonos, “Affordance detection of tool parts from geometric features,” in *Proc. ICRA*, 2015, pp. 1374–1381.
- [6] H. Luo, W. Zhai, J. Zhang, Y. Cao, and D. Tao, “Learning affordance grounding from exocentric images,” in *Proc. CVPR*, 2022, pp. 2242–2251.
- [7] G. Li, V. Jampani, D. Sun, and L. Sevilla-Lara, “LOCATE: Localize and transfer object parts for weakly supervised affordance grounding,” in *CVPR*, 2023, pp. 10 922–10 931.
- [8] Y. Wei *et al.*, “AffordDexGrasp: Open-set language-guided dexterous grasp with generalizable-instructive affordance,” in *Proc. ICCV*, 2025, pp. 11 818–11 828.
- [9] Y. Zhang *et al.*, “FunctionalGrasp: Learning functional grasp for robots via semantic hand-object representation,” *IEEE Robotics and Automation Letters*, vol. 8, no. 5, pp. 3094–3101, 2023.
- [10] F. Yang *et al.*, “Multi-keypoint affordance representation for functional dexterous grasping,” *IEEE Robotics and Automation Letters*, vol. 10, no. 10, pp. 10 306–10 313, 2025.
- [11] S. Wang, W. Hu, L. Sun, X. Wang, and Z. Li, “Learning adaptive grasping from human demonstrations,” *IEEE/ASME Transactions on Mechatronics*, vol. 27, no. 5, pp. 3865–3873, 2022.

- [12] X. Xu, M. You, H. Zhou, Z. Qian, and B. He, "Robot imitation learning from image-only observation without real-world interaction," *IEEE/ASME Transactions on Mechatronics*, vol. 28, no. 3, pp. 1234–1244, 2023.
- [13] G. Li *et al.*, "Learning precise affordances from egocentric videos for robotic manipulation," in *Proc. ICCV*, 2025, pp. 10 581–10 591.
- [14] F. Yang *et al.*, "Task-oriented tool manipulation with robotic dexterous hands: A knowledge graph approach from fingers to functionality," *IEEE Transactions on Cybernetics*, vol. 55, no. 1, pp. 395–408, 2025.
- [15] B. Zitkovich *et al.*, "RT-2: Vision-language-action models transfer web knowledge to robotic control," in *Proc. CoRL*, vol. 229, 2023, pp. 2165–2183.
- [16] Y. Yue *et al.*, "DeeR-VLA: Dynamic inference of multimodal large language models for efficient robot execution," in *Proc. NeurIPS*, vol. 37, 2024, pp. 56 619–56 643.
- [17] J. Liu *et al.*, "RoboMamba: Efficient vision-language-action model for robotic reasoning and manipulation," in *Proc. NeurIPS*, vol. 37, 2024, pp. 40 085–40 110.
- [18] J. Wen *et al.*, "DiffusionVLA: Scaling robot foundation models via unified diffusion and autoregression," in *Proc. ICML*, 2025.
- [19] J. He *et al.*, "DexVLG: Dexterous vision-language-grasp model at scale," *arXiv preprint arXiv:2507.02747*, 2025.
- [20] Y. Chen *et al.*, "Towards human-level bimanual dexterous manipulation with reinforcement learning," in *Proc. NeurIPS*, vol. 35, 2022, pp. 5150–5163.
- [21] W. Huang, C. Wang, Y. Li, R. Zhang, and L. Fei-Fei, "ReKep: Spatio-temporal reasoning of relational keypoint constraints for robotic manipulation," in *Proc. CoRL*, vol. 270, 2024, pp. 4573–4602.
- [22] Z. Li *et al.*, "Language-guided dexterous functional grasping by LLM generated grasp functionality and synergy for humanoid manipulation," *IEEE Transactions on Automation Science and Engineering*, vol. 22, pp. 10 506–10 519, 2025.
- [23] H. Zhu *et al.*, "Grounding 3D object affordance with language instructions, visual observations and interactions," in *Proc. CVPR*, 2025, pp. 17 337–17 346.
- [24] X. Yao *et al.*, "Long-horizon language-conditioned imitation learning for robotic manipulation," *IEEE/ASME Transactions on Mechatronics*, vol. 30, no. 6, pp. 5628–5639, 2025.
- [25] W. Shen, G. Yang, A. Yu, J. Wong, L. P. Kaelbling, and P. Isola, "Distilled feature fields enable few-shot language-guided manipulation," in *Proc. CoRL*, vol. 229, 2023, pp. 405–424.
- [26] B. Kerbl, G. Kopanas, T. Leimkühler, and G. Drettakis, "3D gaussian splatting for real-time radiance field rendering," *ACM Transactions on Graphics (TOG)*, vol. 42, no. 4, pp. 1–14, 2023.
- [27] Y. Zheng *et al.*, "GaussianGrasper: 3D language gaussian splatting for open-vocabulary robotic grasping," *IEEE Robotics and Automation Letters*, vol. 9, no. 9, pp. 7827–7834, 2024.
- [28] M. Ji, R.-Z. Qiu, X. Zou, and X. Wang, "GraspSplats: Efficient manipulation with 3D feature splatting," in *Proc. CoRL*, vol. 270, 2024, pp. 1443–1460.
- [29] M. Ahn *et al.*, "Do as I can, not as I say: Grounding language in robotic affordances," in *Proc. CoRL*, vol. 205, 2022, pp. 287–318.
- [30] S. Yu, D.-H. Zhai, and Y. Xia, "Robotic grasp detection based on category-level object pose estimation with self-supervised learning," *IEEE/ASME Transactions on Mechatronics*, vol. 29, no. 1, pp. 625–635, 2024.
- [31] S. Srivastava, E. Fang, L. Riano, R. Chitnis, S. Russell, and P. Abbeel, "Combined task and motion planning through an extensible planner-independent interface layer," in *Proc. ICRA*, 2014, pp. 639–646.
- [32] S. Tyree *et al.*, "6-DoF pose estimation of household objects for robotic manipulation: An accessible dataset and benchmark," in *Proc. IROS*, 2022, pp. 13 081–13 088.
- [33] B. Wen, W. Yang, J. Kautz, and S. Birchfield, "FoundationPose: Unified 6D pose estimation and tracking of novel objects," in *Proc. CVPR*, 2024, pp. 17 868–17 879.
- [34] S. Brahmhatt, C. Ham, C. C. Kemp, and J. Hays, "ContactDB: Analyzing and predicting grasp contact via thermal imaging," in *Proc. CVPR*, 2019, pp. 8709–8719.
- [35] H. Cao, G. Chen, Z. Li, Q. Feng, J. Lin, and A. Knoll, "Efficient grasp detection network with gaussian-based grasp representation for robotic manipulation," *IEEE/ASME Transactions on Mechatronics*, vol. 28, no. 3, pp. 1384–1394, 2023.
- [36] F.-J. Chu, R. Xu, and P. A. Vela, "Real-world multiobject, multigrasp detection," *IEEE Robotics and Automation Letters*, vol. 3, no. 4, pp. 3355–3362, 2018.
- [37] J. Lundell, F. Verdoja, and V. Kyrki, "DDGC: Generative deep dexterous grasping in clutter," *IEEE Robotics and Automation Letters*, vol. 6, no. 4, pp. 6899–6906, 2021.
- [38] C. Choi, W. Schwarting, J. DelPreto, and D. Rus, "Learning object grasping for soft robot hands," *IEEE Robotics and Automation Letters*, vol. 3, no. 3, pp. 2370–2377, 2018.
- [39] J. Hang *et al.*, "DexFuncGrasp: A robotic dexterous functional grasp dataset constructed from a cost-effective real-simulation annotation system," in *Proc. AAAI*, 2024, pp. 10 306–10 313.
- [40] A. Radford *et al.*, "Learning transferable visual models from natural language supervision," in *Proc. ICML*, 2021, pp. 8748–8763.
- [41] A. Kirillov *et al.*, "Segment anything," in *Proc. ICCV*, 2023, pp. 3992–4003.
- [42] J. Redmon, S. K. Divvala, R. B. Girshick, and A. Farhadi, "You only look once: Unified, real-time object detection," in *Proc. CVPR*, 2016, pp. 779–788.
- [43] R. Raguram, O. Chum, M. Pollefeys, J. Matas, and J.-M. Frahm, "USAC: A universal framework for random sample consensus," *IEEE Transactions on Pattern Analysis and Machine Intelligence*, vol. 35, no. 8, pp. 2022–2038, 2013.
- [44] A. Maćkiewicz and W. Ratajczak, "Principal components analysis (PCA)," *Computers & Geosciences*, vol. 19, no. 3, pp. 303–342, 1993.
- [45] F. Yang *et al.*, "Learning granularity-aware affordances from human-object interaction for tool-based functional dexterous grasping," *IEEE Transactions on Neural Networks and Learning Systems*, vol. 36, no. 11, pp. 19 589–19 603, 2025.
- [46] J. Achiam *et al.*, "GPT-4 technical report," *arXiv preprint arXiv:2303.08774*, 2023.
- [47] A. Liu *et al.*, "DeepSeek-V3 technical report," *arXiv preprint arXiv:2412.19437*, 2024.
- [48] G. Comanici *et al.*, "Gemini 2.5: Pushing the frontier with advanced reasoning, multimodality, long context, and next generation agentic capabilities," *arXiv preprint arXiv:2507.06261*, 2025.
- [49] C. Chi *et al.*, "Diffusion policy: Visuomotor policy learning via action diffusion," *The International Journal of Robotics Research*, vol. 44, no. 10-11, pp. 1684–1704, 2025.